Multicolor Conjugated Polymer Dots for Biological Fluorescence Imaging

Changfeng Wu, Barbara Bull, Craig Szymanski, Kenneth Christensen, and Jason McNeill*

Department of Chemistry and Center for Optical Materials Science and Engineering Technologies, Clemson University, Clemson, South Carolina 29634

ABSTRACT Highly fluorescent conjugated polymer dots were developed for demanding applications such as fluorescence imaging in live cells. These nanoparticles exhibit small particle diameters, extraordinary fluorescence brightness, and excellent photostability. Single particle fluorescence imaging and kinetic studies indicate much higher emission rates ($\sim 10^8$ s^{-1}) and little or no blinking of the nanoparticles as compared to typical results for single dye molecules and quantum dots. Analysis of single particle photobleaching trajectories reveals excellent photostability—as many as 10^9 or more photons emitted per nanoparticle prior to irreversible photobleaching. The superior figures of merit of these new fluorescent probes, together with the demonstration of cellular imaging, indicate their enormous potential for demanding fluorescence-based imaging and sensing applications such as high speed super-resolution single molecule/particle tracking and highly sensitive assays.

KEYWORDS: conjugated polymer dots · fluorescent probes · single molecule · nanoparticle · fluorescence imaging

Recent developments in fluorescence spectroscopy and microscopy coupled with bioconjugation techniques are leading to a rapid proliferation of advanced fluorescence-based techniques in chemistry and the life sciences. In particular, fluorescence-based methods for probing biomolecular interactions at the single molecule level have resulted in significant advances in our understanding of various biochemical processes.[1] The extension of single molecule fluorescence methods to living cells promises to provide an unprecedented understanding about cellular processes such as gene expression, protein transport, signaling, and regulatory processes.[2−5] However, the application of single molecule methods to a broad range of processes in living cells is hindered by the current lack of dyes that are sufficiently bright and photostable to overcome the background fluorescence and scattering within the cell. A useful estimate of fluorescence brightness is given by the product of the peak absorption cross section and the fluorescence quantum yield—typical fluorescent dyes employed in fluorescence microscopy exhibit absorption cross sections in the range of 10^{-16}−10^{-17} cm^2 and fluorescence quantum yields ranging from a few percent to nearly 100%. The limited brightness of conventional dyes and cellular autofluorescence results in signal-to-background ratios that are too low for single molecule fluorescence detection. The photostability of fluorescent probes is also critically important for single molecule imaging and tracking. The most photostable dyes such as Rhodamine 6G can emit only $\sim 10^6$ photons prior to irreversible photobleaching,[6] insufficient for long-term single molecule fluorescence tracking. In addition, fluorescence intermittency ("blinking") of fluorescent dyes can complicate single molecule measurements.

A number of strategies for developing brighter fluorescent probes have been pursued. Green fluorescent proteins (GFP) and some derivatives can in favorable cases be detected at the single molecule level.[7] However, approximately 30 copies of GFP are required for long-term single molecule tracking inside cells.[8] Fluorescent nanoparticles such as colloidal semiconductor quantum dots are under active development.[9,10] However, these nanoparticles typically require an inorganic shell and a thick encapsulation layer to reach the required levels of stability and biocompatibility, resulting in larger diameters which can significantly alter biological function and transport of the biomolecules. While there has been recent work to reduce the thickness of the biocompatibility and encapsulation layers,[11] low emission rates, blinking, and a significant fraction of "dark" particles continue to pose potential difficulties for single particle measurements.[12] Dye-loaded latex or silica beads also possess relatively large sizes (>20 nm)[13] and limited dye-loading

*Address correspondence to mcneill@clemson.edu.

Received for review September 17, 2008 and accepted October 28, 2008.

Published online November 7, 2008.
10.1021/nn800590n CCC: $40.75

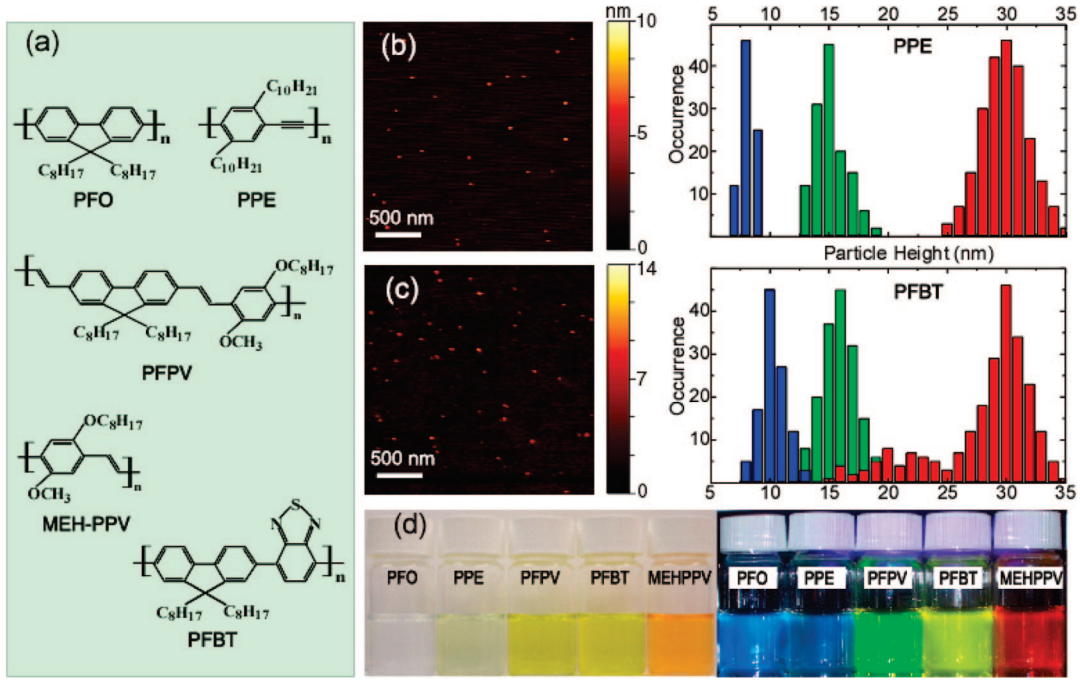

Figure 1. (a) Chemical structures of fluorescent conjugated polymer dots; (b) typical AFM image of small PPE dots and histograms of particle height of the PPE dots prepared with different precursor concentration; (c) typical AFM image of small PFBT dots and histograms of particle height of the PFBT dots prepared with different precursor concentrations; (d) photographs of aqueous CPdot suspensions under room light (left) and UV light (right) illumination.

concentration due to aggregation and self-quenching.

These limitations of current luminescent particles provide clear motivation for exploring alternative strategies for the design of more highly fluorescent nanoparticles. One promising strategy is the development of nanoparticles based on highly fluorescent π-conjugated polymers. There has been steady progress in the development of highly fluorescent π-conjugated polymers as the active material in polymer light-emitting devices.[14,15] Conjugated polyelectrolytes have also been demonstrated for application as highly sensitive biosensors.[16,17] We recently developed conjugated polymer nanoparticles (CPdots) that are small (diameters as low as ~4 nm), exhibit extraordinarily high fluorescence brightness under both one-photon and two-photon excitation, and can be encapsulated and functionalized.[18,19] CPdots possess arguably the highest fluorescence brightness/volume ratios of any nanoparticle to date, owing to a number of favorable characteristics of conjugated polymer molecules, including their high absorption cross sections (typically 10^{-15}~10^{-14} cm^2), high radiative rates, high effective chromophore density, and minimal levels of aggregation-induced fluorescence quenching, resulting in fluorescence quantum yields in excess of 70%, even for pure solid films.[20] The use of conjugated polymers as the active material also confers other useful advantages, such as the lack of small dye molecules or heavy metal ions that could leach out into solution.

In this article, we explore the size-controlled preparation of several new polymer dots and their photophysical characteristics relevant for demanding applications such as single particle tracking. These new polymer dots show remarkable improvements in terms of their fluorescence quantum yield, radiative rate, and photostability as compared to those in our previous reports.[18,19] Single particle imaging, photobleaching kinetics, and fluorescence saturation studies indicate much higher emission rates (~10^8 s^{-1}) and little or no blinking of the CPdots as compared to typical results for single dye molecules and colloidal semiconductor quantum dots. Analysis of photobleaching trajectories for some polymer dots indicates excellent photostability—as many as 10^9 or more photons emitted per nanoparticle prior to irreversible photobleaching. Cellular uptake of the nanoparticles *via* endocytosis was observed. The extraordinary brightness of the CPdots, high emission rates, small particle diameters, and the demonstration of cellular uptake indicate that CPdots are promising probes for demanding fluorescence applications such as high speed super-resolution single molecule/particle tracking and highly sensitive assays.

RESULTS AND DISCUSSION

Figure 1a provides the chemical structures and acronyms of the conjugated polymers employed in this study (see Experimental Methods for the full names of polymers). Multicolored CPdots were prepared using the reprecipitation procedure described previously.[18] The procedure involves a rapid injection of a hydrophobic polymer in tetrahydrofuran (THF) solution into wa-

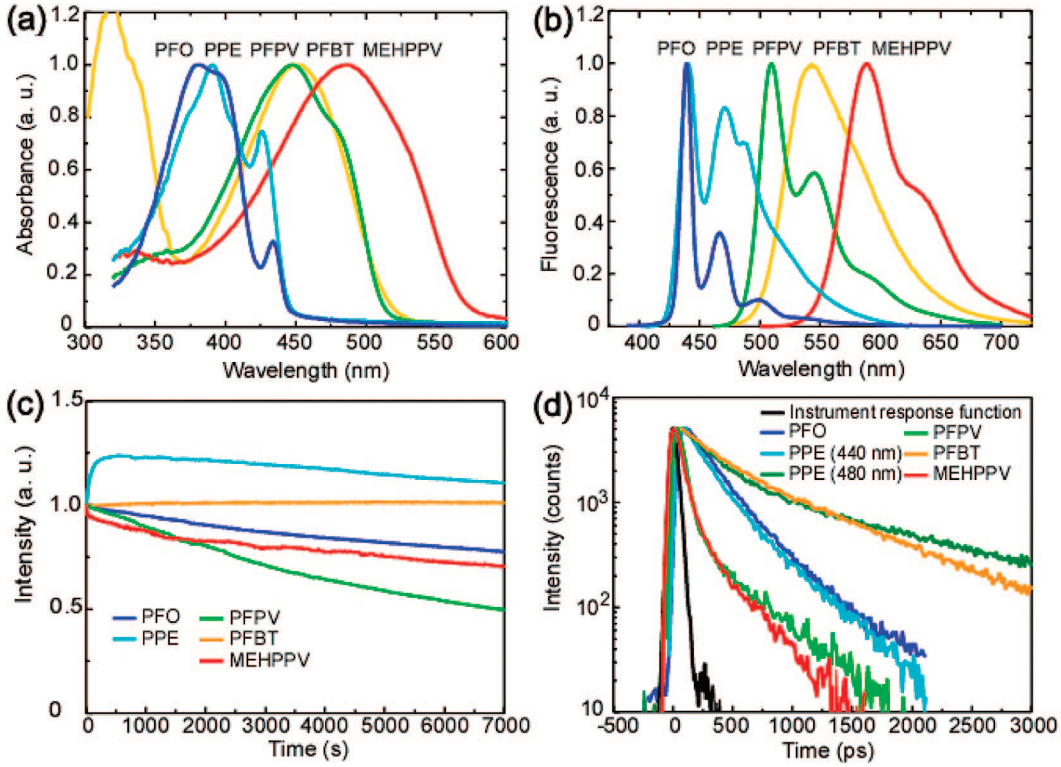

Figure 2. Absorption spectra (a), fluorescence spectra (b), photobleaching curves (c), and fluorescence decay traces (d) of various conjugated polymer dots.

ter, while applying sonication to improve mixing. The sudden decrease in solution hydrophobicity leads to collapse of polymer chains, resulting in the formation of hydrophobic polymer nanoparticles. Since the reprecipitation process involves a competition between aggregation and chain collapse to form nanoparticles, the particle size can be controlled by adjusting the polymer concentration in the precursor solution. To explore the effect of precursor concentration on particle size, we focus our discussion on two polymers that form highly photostable nanoparticles: PPE and PFBT. PPE dots were prepared using different concentrations of the polymer in the precursor solution ranging from 20 to 2000 ppm (see Experimental Methods for details). As shown in the AFM image of Figure 1b, the PPE nanoparticles exhibit an approximately spherical shape. Analysis of particle height indicates that the nanoparticles produced using the lowest precursor concentration possess small particle size and a relatively narrow size distribution (8 $\pm$ 1 nm diameter), while those prepared from more concentrated precursor solutions exhibited larger diameters. PFBT dots that were also prepared using a range of concentrations of the precursor solution exhibit a similar trend—the PFBT dots obtained using a dilute solution exhibit relatively small particle size and size distribution (10 $\pm$ 3 nm), while those prepared using higher precursor concentrations exhibit larger size (Figure 1d). The preparation of small particles of both PPE and PFBT polymers are consistent with our previous reports on PDHF, PFPV, and MEH-PPV particles.[18]

The specific particle size and size distribution are also dependent on the polymer species (as well as other conditions that may affect the mixing and aggregation rates). For example, the larger PFBT dots in Figure 1c exhibit a relatively broad size distribution (25 $\pm$ 10 nm) and a substantial fraction of small dots. PFPV dots prepared under the same conditions exhibited much larger particle sizes, in the range of 50−70 nm. The size differences are likely due to differences in the molecular weight, polydispersity, and interchain interactions of the different polymers. It was also found that the preparation conditions affect the polymer phase for PFO polymer, with a fraction of β-phase formed under certain conditions.[21]

The aqueous CPdot suspensions obtained from various conjugated polymers are stable and clear (not turbid), presenting colors associated with their visible absorption spectra. Under UV lamp illumination (365 nm), the nanoparticle dispersions exhibit strong fluorescence with a wide variety of colors, as shown in Figure 1d. The changes in the absorption spectra and fluorescence spectra upon particle formation vary depending on the polymer (Figure 2, top). For PFBT, PFPV, and MEHPPV, the absorption spectra are broadened and blue-shifted as compared to those of the polymer in THF solution, which is consistent with an overall decrease in the conjugation length due to bending, torsion, and kinking of the polymer backbone. The nanoparticles also (in most cases) exhibit a slightly red-shifted fluorescence and a long red tail as compared to the polymer

TABLE 1. Figures of Merit Evaluating the Multicolor Conjugated Polymer Dots as Fluorescent Tags

CPdots (ave diameter 15 nm) (absorption/fluorescence max, nm)	PFO (380/435)	PPE (390/440)	PFPV (445/510)	PFBT (450/545)	MEHPPV (485/590)
absorption cross section (σ, cm^2)	5.4×10^{-13}	4.6×10^{-13}	5.5×10^{-13}	2.8×10^{-13}	4.4×10^{-13}
quantum yield (ϕ_F)	0.40	0.12	0.08	0.07	0.01
fluoresence lifetime (τ, ps)	270	242	133	595	127
radiative rate (k_r, s^{-1})	1.5×10^9	5.0×10^8	6.0×10^8	1.2×10^8	7.9×10^7
photobleaching quantum yield (ϕ_B)	$\sim 10^{-8}$	$\sim 10^{-9}$	$\sim 10^{-8}$	$\sim 10^{-10}$	$\sim 10^{-8}$
photon number (photons)	$\sim 10^7$	$\sim 10^8$	$\sim 10^7$	$\sim 10^9$	$\sim 10^6$

in organic solvent. This is attributable to increased interchain interactions due to chain collapse, resulting in a fraction of red-shifted aggregate species.[18] The resulting energetic disorder, combined with multiple energy transfer, would result in a net red-shift in the fluorescence spectrum as compared to that of the polymer in THF solution, as has often been observed in thin films.[22] For PFO nanoparticles, the additional absorption feature and the red-shifted fluorescence are attributed to the β-phase conformation.[21] The relatively complex absorption and fluorescence structures observed for PPE dots may be due to the complex packing and phase behavior of polymer chains, as was previously observed in thin films of similar PPE derivatives.[23] However, due to the complex phase behavior of PPE derivatives, additional studies are required to obtain definitive information about the internal structure of the nanoparticles.

CPdots exhibit broad absorption bands ranging from 350 to 550 nm (depending on the polymer), a wavelength range that is convenient for fluorescence microscopy and laser excitation. Analysis of the UV−vis absorption spectra at a known particle concentration indicated that the peak absorption cross section of single particles (~15 nm diameter) was on the order of $\sim 10^{-13}$ cm^2, roughly 10−100 times larger than that of CdSe quantum dots in the visible and near-UV range, and roughly 3 orders of magnitude larger than typical organic fluorescent dyes. Fluorescence quantum yields (ϕ_F) ranged from a few percent to as high as 40%, depending on the polymer. The absorption cross section and quantum yield results are summarized in Table 1. These results indicate that, to the best of our knowledge, the fluorescence brightness of the CPdot nanoparticles exceeds that of any other nanoparticle of the same size under typical conditions. The size of the particle does not appear to have an appreciable effect on the shape of the absorption and fluorescence spectra—the principal effect of increased particle size is an increase in the absorption cross section. This property facilitates adjustment of particle size and brightness to meet the demands of a particular application and is in contrast with colloidal semiconductor quantum dots, which exhibit pronounced variations in band gap due to the quantum size effect. For a given polymer, particle size was also found to affect fluorescence quantum yield. For example, a quantum yield of ~0.10 was determined for small PFPV dots (~10 nm), while larger PFPV particles (~60 nm) exhibit a decreased quantum yield of ~0.04. The size dependence of the quantum yield is likely due to the effect of particle size on the efficiency of energy transfer to various fluorescence quencher species present in the nanoparticle, consistent with both the results of exciton diffusion and energy transfer simulations and the size-dependent energy transfer efficiency we have previously observed in dye-doped CPdots.[24] The effect of particle size on exciton−phonon coupling may also play a role.[25]

The photostability of the CPdot nanoparticles is critically important for many fluorescence-based imaging applications, particularly for long-term imaging and tracking experiments.[26] The photostability of a fluorescent dye or nanoparticle can be characterized by photobleaching quantum yield (ϕ_B), which is the number of molecules that have been photobleached divided by the total number of photons absorbed over a given time interval. Typical fluorescent dyes exhibit photobleaching quantum yields in the range of 10^{-4} to 10^{-6},[6] and exhibit single exponential photobleaching kinetics under low excitation intensity. The photobleaching of conjugated polymers is more complicated due to the complex set of interactions involving a large number of species such as excitons, polarons, molecular oxygen, and fluorescence-quenching sites of unknown structure.[27−29] Photobleaching kinetics of the aqueous CPdot suspensions were observed to vary substantially from one polymer to another (Figure 2c). While PFO and PFPV dots exhibit single exponential photobleaching decays, the photobleaching kinetics of MEH-PPV dots contain a fast component and a slow component. The PPE dots exhibit unusual photobleaching behavior: initial light excitation increases the fluorescence quantum yield, resulting in a rapid increase in fluorescence followed by slow photobleaching. The PFBT dots appear to be remarkably photostable—photobleaching for 2 h does not result in observable decrease in fluorescence intensity. These observations indicate complex photophysics in these nanoscale multichromophoric systems, and more detailed investigations are needed to better understand how these phenomena are determined by the polymer structure and environment. An estimate of both the photobleaching quantum yield and the photon number (total number of photons that a particle emits prior to photobleaching) can be obtained from the rate constants obtained from the photobleaching kinetics measurements.[6] As shown in Table 1, the photon numbers of the CPdots are 3−4 orders of magnitude larger than those of typical fluorescent dyes,[6] indicating promise for long-term imaging and tracking applications.

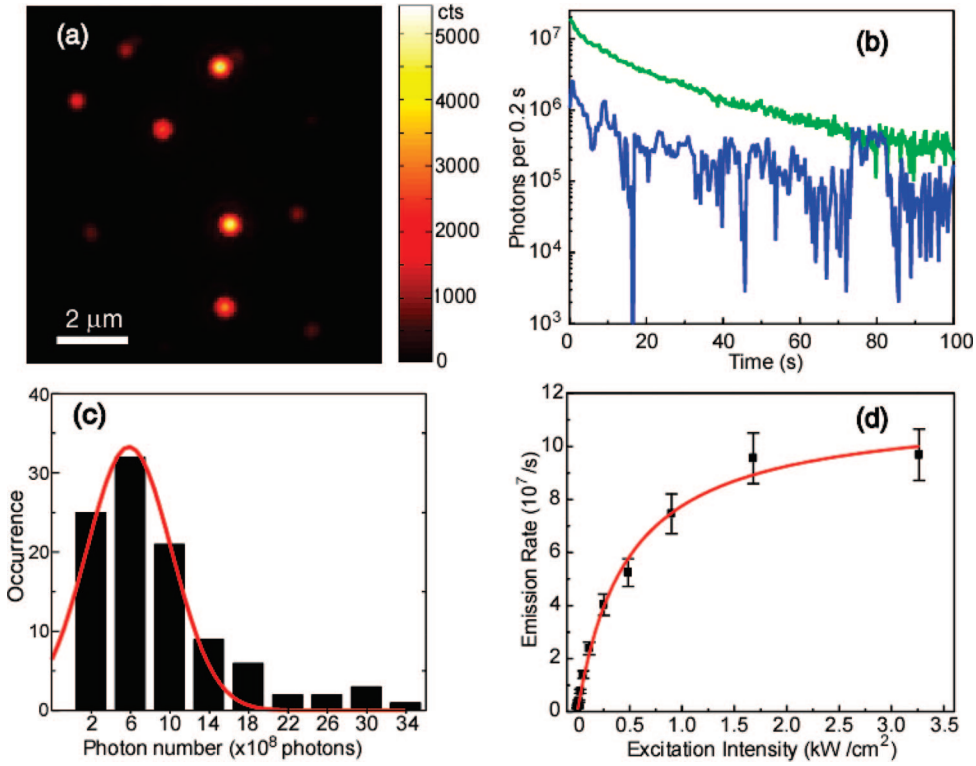

Figure 3. (a) A 10 μm × 10 μm fluorescence image of single PFBT dots immobilized on a glass coverslip. (b) Photobleaching trajectories of single PFBT dots. No obvious blinking was observed for larger PFBT dots (green), while it was sometimes observed for smaller particles (blue). (c) Histogram of the photon numbers of several individual PFBT dots (~10 nm) prior to irreversible photobleaching. (d) Fluorescence saturation of single PFBT dots with increasing excitation intensity. The scattered points are experimental data, while the solid curve represents a fit to the saturation equation $R = R_\infty(I/I_s)(1 + I/I_s)^{-1}$.

For high-speed applications, such as flow cytometry and high-speed imaging and tracking, a key figure of merit is the fluorescence radiative rate. Fluorescence decay kinetics (Figure 2d) were obtained using the time-correlated single photon counting technique (TCSPC), and excited-state lifetimes were extracted from the kinetics traces using custom software. All decay traces of the CPdots (with the exception of the 480 emission band of PPE dots) can be fit adequately with a single exponential function, and the lifetime results are listed in Table 1. The lifetimes of PFPV and MEHPPV dots were determined to be ~130 ps, while β-phase PFO and PFBT dots show longer lifetimes around ~270 and ~600 ps, respectively. PPE dots display complex fluorescence decay kinetics, the 440 nm emission peak shows a single exponential decay with time constant of 242 ps, while the 480 nm emission exhibits a biexponential decay with time constants of 276 ps and 1.56 ns. This observation is similar to previously observed fluorescence decay kinetics of PPE thin films, which are characterized as a heterogeneous system containing ordered and disordered polymer chains.[23] The fluorescence radiative rate constant k_R and nonradiative rate constant k_{NR} were estimated by combining the quantum yield [$\phi = k_R/(k_R + k_{NR})$] and fluorescence lifetime results [$\tau = (k_R + k_{NR})^{-1}$]. Typical fluorescent dyes exhibit fluorescence radiative rates on the order of ~10^8 s^{-1}. As shown in Table 1, the CPdots exhibit a fluorescence radiative rate (10^8–10^9 s^{-1}) similar to or somewhat higher than that of typical fluorescent dyes, while single quantum dots emit at rates about 2 orders of magnitude lower.[30] The fluorescence radiative rates of the CPdots are at or above those of other fluorophores used in flow cytometry and imaging.

Single particle fluorescence imaging and kinetics studies provide further evidence of the CPdots as fluorescent probes for single molecule applications. Photobleaching studies of single PFBT dots (particle size = 10 ± 3 nm) dispersed on a glass coverslip were performed using a custom-built wide-field epifluorescence microscope. Bright, near-diffraction-limited spots corresponding to individual PFBT dots were observed (Figure 3a). Single particle photobleaching measurements were obtained by acquiring a series of consecutive frames. The number of fluorescence photons emitted per frame for a given particle was estimated by integrating the CCD signal over the fluorescence spot and then scaling that value with the detection efficiency and amplification factor of the detector and the overall collection efficiency of the microscope. The photobleaching trajectories could be roughly categorized into two types exemplified by the curves shown in Figure 3b. Most of the particles exhibit continuous photobleaching behavior with no observable fluorescence blinking, as indicated by the green curve, while some blinking was often observed in dimmer particles (blue curve). This is

consistent with the size-dependent blinking observed in other conjugated polymers:[19,31] the fluorescence of the smaller (dimmer) particles fluctuates due to the small number of emitting chromophores and the reversible on−off dynamics resulting in sizable fluctuations in the fraction of chromophores in the "on" state; while larger particles (>10 nm diameter) result in relatively steady fluorescence, there are contributions from a larger number of chromophores, resulting in smaller fluctuations. As fluorescent probes for imaging or single particle tracking, the steady fluorescence of the larger CPdots compares favorably to that of conventional dyes and quantum dots, which often exhibit pronounced blinking on time scales of microseconds to hundreds of seconds,[12] although such blinking can be suppressed in some cases.[32] Statistical analyses of multiple photobleaching trajectories indicate that approximately ~6 × 10^8 photons per particle (~10 nm diameter) were emitted prior to photobleaching (Figure 3c). The average photon number (number of photons emitted prior to photobleaching) obtained from single particle measurements is roughly consistent with the bulk photobleaching results (given an estimated uncertainty of ~20% in the determined photon number). Additional photobleaching experiments performed under nitrogen resulted in photon numbers roughly 2 orders of magnitude higher, indicating that oxygen is likely involved in the photobleaching mechanism (data not shown).

In single molecule experiments and other measurements involving high excitation intensities, the emission rate is often determined by saturation due to the presence of triplets and other long-lived nonfluorescent species. Typical fluorescent dyes exhibit a saturated emission rate on the order of 10^6 s^{-1} due to triplet saturation.[33] This picture is complicated for multichromophoric systems such as conjugated polymers, as evidenced by photon antibunching studies and single molecule blinking studies that indicate roughly between one and three independent emitters for single conjugated polymer chains.[34,35] This value is much lower than the chromophore number that is expected based on the extinction coefficients and conjugation lengths of conjugated polymers, and the discrepancy can be attributed to funneling of excitons to a small number of emitters. Fluorescence saturation studies of single PFBT dots were performed under nitrogen protection so that photobleaching was negligible (however, the absence of oxygen also tends to increase triplet lifetimes, resulting in increased triplet saturation[36]). As shown in Figure 3d, the fluorescence signal of a PFBT particle shows power saturation behavior that is well described by the saturation equation $R = R_\infty(I/I_s)(1 + I/I_s)^{-1}$, where I and I_s are the excitation and the saturation intensities, respectively. From the fit of this particle, we obtain a saturation emission rate $R_\infty = 1.1 \times 10^8$ s^{-1} and $I_s = 0.5$ kW · cm^{-2}. Statistical analysis of several particles yielded saturation emission rates ranging from 10^7 to 10^9 s^{-1}. The mean saturation emission rate is roughly 100 times higher than that of typical molecular dyes, and at least 3 orders of magnitude higher than that of colloidal semiconductor quantum dots. The single particle saturation emission rate is markedly lower than the expected per-particle radiative rate based on the results of prior single molecule studies and the number of polymer chains per nanoparticle (~40). This apparent discrepancy is likely due to the larger number of available pathways for exciton diffusion in the nanoparticles relative to single conjugated polymer molecules, resulting in additional energy funneling.

The high absorption cross sections, bright fluorescence, and large photon numbers of the CPdots indicate great potential for single molecule imaging and tracking in living cells. As compared to membrane-permeable organic dyes, the use of nanoparticles for intracellular imaging is generally complicated by the challenge of delivering the nanoparticles to the interior of the cell.[37] A variety of strategies including invasive methods such as electroporation and microinjection have been demonstrated for intracellular delivery of inorganic quantum dots.[38] Here we demonstrate the effective use of CPdots as an extremely bright fluid phase marker of pinocytosis in J774.A1 macrophages. The selection of the cell system is based on the ability of macrophages to efficiently ingest cellular debris, pathogens, and small particles such as CPdots. Figure 4 shows differential interference contrast (DIC) images and fluorescence images of these mouse macrophage-like cells that had been incubated with PPE, PFPV, PFBT, and MEH-PPV dots, respectively. These images clearly indicate internalization of the CPdots by the cells and show a staining pattern consistent with other widely used fluid-phase markers such as an organic dye conjugated to a high molecular weight dextran. Consistent with fluid-phase uptake of CPdots, these representative images show perinuclear labeling and brightly fluorescent vacuoles and organelles (*e.g.*, pinosomes and lysosomes). Preliminary colocalization studies with Texas Red dextran and Lysotracker Red favor fluid-phase uptake as the most likely primary uptake mechanism. More diffuse nanoparticle fluorescence was observed in the cytoplasm, possibly indicating that some of the CPdots crossed cell membranes. The CPdots do not appear to exhibit appreciable cytotoxicity under the current incubation time and loading concentration. The nanoparticles also appear to be stable (no evidence of degradation) in cell growth medium. A detailed understanding of the factors affecting nanoparticle uptake as well as the fate of the nanoparticles requires additional investigation. In addition, imaging or tracking specific intracellular species will require targeting of the CPdots *via* encapsulation and bioconjugation.

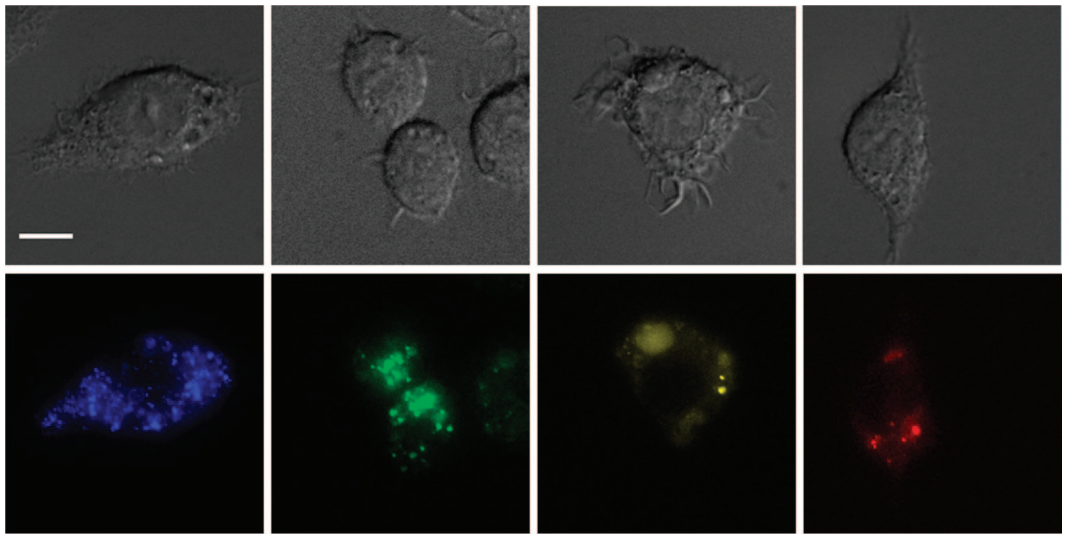

Figure 4. Differential interference contrast (DIC) images (top), and fluorescence images (bottom) of macrophage cells labeled with macrophage cells labeled with PPE, PFPV, PFBT, and MEHPPV dots, respectively. Scale bar: 10 μm.

CONCLUSIONS

In conclusion, we report on a variety of CPdot nanoparticles which are promising for demanding fluorescence applications such as single molecule tracking in live cells. Preparation of CPdot nanoparticles with reasonably well-controlled size distributions was demonstrated. Nanoparticle absorption cross section of $\sim 10^{-13}$ cm^2 and fluorescence quantum yields as high as ~40% have been determined for some CPdots. The fast radiative rates of conjugated polymers and the large number of densely packed chromophores result in much higher emission rates and minimal "blinking" behavior under single particle imaging conditions as compared to other nanoparticles in this size range. The nanoparticles also exhibit excellent photostability, with photon numbers exceeding 10^9 in some cases (even higher when oxygen is excluded). Nanoparticle uptake *via* endocytosis was observed in live macrophage cells. The superior figures of merit of the CPdots—in particular, the exceptional brightness and excellent photostability of nanoparticles with diameters in the range of 5−15 nm—together with the demonstration of cellular imaging, indicate their enormous potential for demanding fluorescence-based imaging and sensing applications such as high speed super-resolution single molecule/particle tracking in live cells and highly sensitive assays. CPdots would yield substantially improved signal levels for these photon-starved applications that have previously involved multiple dye labeling, quantum dots, or dye-loaded particles, likely increasing the feasibility of such techniques for a wider range of problems. While the results reported here are highly encouraging, it is likely that additional significant improvements in CPdot optical properties could be achieved by developing and employing conjugated polymers with higher brightness or improved photostability, or by encapsulation or energy transfer schemes.

EXPERIMENTAL METHODS

The polyfluorene derivative poly(9,9-dioctylfluorenyl-2,7-diyl) (PFO, MW 147 000, polydispersity 3.0), the copolymer poly[{9,9-dioctyl-2,7-divinylene-fluorenylene}-*alt*-*co*-{2-methoxy-5-(2-ethylhexyloxy)-1,4-phenylene}] (PFPV, MW 270 000, polydispersity 2.7), poly[(9,9-dioctylfluorenyl-2,7-diyl)-*co*-(1,4-benzo-{2,1′,3}-thiadiazole)] (PFBT, MW 10 000, polydispersity 1.7), and the poly(phenylene vinylene) derivative poly[2-methoxy-5-(2-ethylhexyloxy)-1,4-phenylenevinylene] (MEH-PPV, MW 200 000, polydispersity 4.0) were purchased from ADS Dyes, Inc. (Quebec, Canada). Poly(2,5-di(3′,7′-dimethyloctyl)phenylene-1,4-ethynylene (PPE) and the solvent tetrahydrofuran (THF, anhydrous, 99.9%) were purchased from Sigma-Aldrich (Milwaukee, WI). Coumarin 1 and coumarin 6 were purchased from Exciton (Dayton, OH). All chemicals were used without further purification. For nanoparticle preparation, 20 mg of conjugated polymer was dissolved in 10 g of HPLC grade THF by stirring overnight under inert atmosphere, and the solution was filtered through a 0.7 μm glass fiber filter in order to remove any insoluble material. Three samples of polymer dots were prepared by injecting the polymer in THF solutions (2 mL of 20 ppm, 100 μL of 1000 ppm, and 100 μL of 2000 ppm) to 8 mL of water. The THF was removed by partial vacuum evaporation, and a small fraction of aggregates was removed by filtration through a 0.2 μm membrane filter. Higher precursor concentrations resulted in larger particle sizes.

For the AFM measurements, one drop of the nanoparticle dispersion was placed on a freshly cleaved mica substrate. After evaporation of the water, the surface topography was imaged with an Ambios Q250 multimode AFM in AC mode. UV−vis absorption spectra were recorded with a Shimadzu UV-2101PC scanning spectrophotometer using 1 cm quartz cuvettes. Fluorescence spectra were obtained and photobleaching experiments were conducted using a commercial fluorometer (Quantamaster, PTI, Inc.). Photobleaching measurements were performed using methods similar to those described elsewhere,[6] but using the light source built in the fluorometer. The slit widths on the excitation monochromator of the fluorometer were adjusted slightly to generate illumination light (wavelength corresponding to the peak absorption of each polymer dot) with a power of 1.0 mW as determined by a calibrated photodiode (Newport model 818-sl). The light was focused into a quartz cu-

vette containing constantly stirred CPdot dispersion with an absorbance of 0.10. The fluorescence intensity at a specific wavelength was recorded continuously over a time period of 2 h. Fluorescence lifetimes of the CPdots were measured using time-correlated single-photon counting (TCSPC). The sample was excited by the second harmonic (400 nm, ~100 fs pulses) of a mode-locked femtosecond Ti:sapphire laser (Coherent Mira 9000). The output of a fast PIN diode (Thorlabs, DET210) monitoring the laser pulse was used as the start pulse for a time-to-amplitude converter (TAC, Canberra Model 2145). Fluorescence signal from the aqueous nanoparticle dispersion was collected in perpendicular to the excitation, passed through appropriate emission filters for different CPdots, and detected by a single photon counting module (id Quantique, ID100-50). The output of the detector was used as the stop pulse for the TAC. The laser was attenuated to maintain the count rate below 20 kHz. The signal from the TAC was digitized using a multichannel analyzer (FastComTec, MCA-3A). The instrument response function was measured before and after each fluorescence lifetime measurement using the scattered laser light from a dilute suspension of polystyrene beads. The combination of the detector and electronics results in an instrument response function with a width of ~50 ps (fwhm). Custom software written for the MATLAB environment (Mathworks) employing standard fitting methods was employed to determine the fluorescence lifetime. Statistical analyses yielded an estimated uncertainty in lifetime of 15 ps or better.

For single particle imaging, a dilute suspension of PFBT dots was drop-cast onto a cleaned microscope cover glass. Single particle fluorescence imaging was performed on a customized wide-field epifluorescence microscope described as follows. The 488 nm laser beam from an argon laser is guided onto the epi-illumination port of an inverted fluorescence microscope (Olympus IX-71). Inside the microscope, the laser beam is reflected by a 500 nm long-pass dichroic mirror (Chroma 500 DCLP) and focused onto the back aperture of a high numerical aperture objective (Olympus Ach, 100X, 1.25 NA, Oil). The laser excitation at the sample plane exhibits a Gaussian profile with full width at half-maximum of ~5 μm. Typical laser intensities employed were approximately 500 W/cm^2 in the center of the laser spot in the sample plane. Fluorescence from CPdots is collected by the same objective lens and filtered by the combination of two 500 nm long-pass filters, then refocused by an additional lens onto a back-illuminated frame transfer CCD camera (Princeton Instruments, PhotonMAX: 512B) yielding a pixel resolution of 105 nm/pixel. An overall fluorescence detection efficiency of 3−5% was determined using nile red loaded polystyrene spheres (Molecular Probes).

For cellular imaging, J774.A1 macrophages (ATCC, Manassas, VA) were plated at 2×10^5 cells/dish onto 35 mm glass-bottom microscope dishes (Matek, Ashland, MA) and allowed to incubated overnight (5% CO_2, 37 °C). Next, 300 μL of sterile filtered nanoparticle dispersions (~1 nM) was added to the cells and allowed to incubate for 12 h. The cells were then washed three times with warm Ringer's buffer before viewing. Images were acquired on an inverted microscope (Olympus IX71) using Xe arc lamp excitation and appropriate filters and beamsplitters (Chroma).

Acknowledgment. The authors gratefully acknowledge financial support from the NSF/EPSCoR under Grant Nos. 2001RII-EPS-0132573 and 2004RII-EPS-0447660, NSF CAREER Grant No. CHE-0547846, NIH Grant No. 1R01GM081040, and NSF EFRI Grant No. ENG-0736007.

REFERENCES AND NOTES

1. Moerner, W. E. New Directions in Single-Molecule Imaging and Analysis. *Proc. Natl. Acad. Sci. U.S.A.* **2007**, *104*, 12596–12602.
2. Ha, T.; Ting, A. Y.; Liang, J.; Caldwell, W. B.; Deniz, A. A.; Chemla, D. S.; Schultz, P. G.; Weiss, S. Single-Molecule Fluorescence Spectroscopy of Enzyme Conformational Dynamics and Cleavage Mechanism. *Proc. Natl. Acad. Sci. U.S.A.* **1999**, *96*, 893–898.
3. Yildiz, A.; Forkey, J. N.; McKinney, S. A.; Ha, T.; Goldman, Y. E.; Selvin, P. R. Myosin V Walks Hand-over-Hand: Single Fluorophore Imaging with 1.5 nm Localization. *Science* **2003**, *300*, 2061–2065.
4. Xie, X. S.; Yu, J.; Yang, W. Y. Perspective—Living Cells as Test Tubes. *Science* **2006**, *312*, 228–230.
5. Abbondanzieri, E. A.; Bokinsky, G.; Rausch, J. W.; Zhang, J. X.; Le Grice, S. F. J.; Zhuang, X. W. Dynamic Binding Orientations Direct Activity of HIV Reverse Transcriptase. *Nature* **2008**, *453*, 184–189.
6. Eggeling, C.; Widengren, J.; Rigler, R.; Seidel, C. A. M. Photobleaching of Fluorescent Dyes under Conditions Used for Single-Molecule Detection: Evidence of Two-Step Photolysis. *Anal. Chem.* **1998**, *70*, 2651–2659.
7. Yu, J.; Xiao, J.; Ren, X. J.; Lao, K. Q.; Xie, X. S. Probing Gene Expression in Live Cells, One Protein Molecule at a Time. *Science* **2006**, *311*, 1600–1603.
8. Golding, I.; Cox, E. C. RNA Dynamics in Live *Escherichia coli* Cells. *Proc. Natl. Acad. Sci. U.S.A.* **2004**, *101*, 11310–11315.
9. Bruchez, M.; Moronne, M.; Gin, P.; Weiss, S.; Alivisatos, A. P. Semiconductor Nanocrystals as Fluorescent Biological Labels. *Science* **1998**, *281*, 2013–2016.
10. Michalet, X.; Pinaud, F. F.; Bentolila, L. A.; Tsay, J. M.; Doose, S.; Li, J. J.; Sundaresan, G.; Wu, A. M.; Gambhir, S. S.; Weiss, S. Quantum Dots for Live Cells, *In Vivo* Imaging, and Diagnostics. *Science* **2005**, *307*, 538–544.
11. Liu, W.; Howarth, M.; Greytak, A. B.; Zheng, Y.; Nocera, D. G.; Ting, A. Y.; Bawendi, M. G. Compact Biocompatible Quantum Dots Functionalized for Cellular Imaging. *J. Am. Chem. Soc.* **2008**, *130*, 1274–1284.
12. Yao, J.; Larson, D. R.; Vishwasrao, H. D.; Zipfel, W. R.; Webb, W. W. Blinking and Nonradiant Dark Fraction of Water-Soluble Quantum Dots in Aqueous Solution. *Proc. Natl. Acad. Sci. U.S.A.* **2005**, *102*, 14284–14289.
13. Wang, L.; Wang, K. M.; Santra, S.; Zhao, X. J.; Hilliard, L. R.; Smith, J. E.; Wu, J. R.; Tan, W. H. Watching Silica Nanoparticles Glow in the Biological World. *Anal. Chem.* **2006**, *78*, 646–654.
14. Friend, R. H.; Gymer, R. W.; Holmes, A. B.; Burroughes, J. H.; Marks, R. N.; Taliani, C.; Bradley, D. D. C.; Dos Santos, D. A.; Bredas, J. L.; Loglund, M.; *et al.* Electroluminescence in Conjugated Polymers. *Nature* **1999**, *397*, 121–128.
15. So, F.; Krummacher, B.; Mathai, M. K.; Poplavskyy, D.; Choulis, S. A.; Choong, V. E. Recent Progress in Solution Processable Organic Light Emitting Devices. *J. Appl. Phys.* **2007**, *102*, 091101-1–091101-21.
16. Chen, L.; McBranch, D. W.; Wang, H. L.; Helgeson, R.; Wudl, F.; Whitten, D. G. Highly Sensitive Biological and Chemical Sensors Based on Reversible Fluorescence Quenching in a Conjugated Polymer. *Proc. Natl. Acad. Sci. U.S.A.* **1999**, *96*, 12287–12292.
17. Fan, C. H.; Wang, S.; Hong, J. W.; Bazan, G. C.; Plaxco, K. W.; Heeger, A. J. Beyond Superquenching: Hyper-Efficient Quenching Energy Transfer from Conjugated Polymers to Gold Nanoparticles. *Proc. Natl. Acad. Sci. U.S.A.* **2003**, *100*, 6297–6301.
18. Wu, C.; Szymanski, C.; McNeill, J. Preparation and Encapsulation of Highly Fluorescent Conjugated Polymer Nanoparticles. *Langmuir* **2006**, *22*, 2956–2960.
19. Wu, C.; Szymanski, C.; Cain, Z.; McNeill, J. Conjugated Polymer Dots for Multiphoton Fluorescence Imaging. *J. Am. Chem. Soc.* **2007**, *129*, 12904–12905.
20. Pei, Q. B.; Yang, Y. Efficient Photoluminescence and Electroluminescence from a Soluble Polyfluorene. *J. Am. Chem. Soc.* **1996**, *118*, 7416–7417.
21. Wu, C.; McNeill, J. Swelling-Controlled Polymmer Phase and Fluorescence Properties in Polyfluorene Nanoparticles. *Langmuir* **2008**, *24*, 5855–5861.
22. Nguyen, T. Q.; Martini, I. B.; Liu, J.; Schwartz, B. J. Controlling Interchain Interactions in Conjugated Polymers: The Effects of Chain Morphology on Exciton-Exciton Annihilation and Aggregation in Meh-Ppv Films. *J. Phys. Chem. B* **2000**, *104*, 237–255.

23. Bunz, U. H. F.; Imhof, J. M.; Bly, R. K.; Bangcuyo, C. G.; Rozanski, L.; Vanden Bout, D. A. Photophysics of Poly [P-(2,5-Didodecylphenylene)Ethynylene] in Thin Films. *Macromolecules* **2005**, *38*, 5892–5896.
24. Wu, C.; Zheng, Y.; Szymanski, C.; McNeill, J. Energy Transfer in a Nanoscale Multichromophoric System: Fluorescent Dye Doped Conjugated Polymer Nanoparticles. *J. Phys. Chem. C* **2008**, *112*, 1772–1781.
25. Onodera, T.; Kasai, H.; Okada, S.; Oikawa, H.; Mizuno, K.; Fujitsuka, M.; Ito, O.; Nakanishi, H. Temperature- and Size-Effects on Optical Properties of Perylene Microcrystals. *Opt. Mater.* **2003**, *21*, 595–598.
26. Levi, V.; Ruan, Q. Q.; Gratton, E. 3-D Particle Tracking in a Two-Photon Microscope: Application to the Study of Molecular Dynamics in Cells. *Biophys. J.* **2005**, *88*, 2919–2928.
27. Park, S. J.; Gesquiere, A. J.; Yu, J.; Barbara, P. F. Charge Injection and Photooxidation of Single Conjugated Polymer Molecules. *J. Am. Chem. Soc.* **2004**, *126*, 4116–4117.
28. Yan, M.; Rothberg, L. J.; Papadimitrakopoulos, F.; Galvin, M. E.; Miller, T. M. Defect Quenching of Conjugated Polymer Luminescence. *Phys. Rev. Lett.* **1994**, *73*, 744–747.
29. Yu, J.; Song, N. W.; McNeill, J. D.; Barbara, P. F. Efficient Exciton Quenching by Hole Polarons in the Conjugated Polymer Meh-Ppv. *Isr. J. Chem.* **2004**, *44*, 127–132.
30. Dahan, M.; Laurence, T.; Pinaud, F.; Chemla, D. S.; Alivisatos, A. P.; Sauer, M.; Weiss, S. Time-Gated Biological Imaging by Use of Colloidal Quantum Dots. *Opt. Lett.* **2001**, *26*, 825–827.
31. Grey, J. K.; Kim, D. Y.; Norris, B. C.; Miller, W. L.; Barbara, P. F. Size-Dependent Spectroscopic Properties of Conjugated Polymer Nanoparticles. *J. Phys. Chem. B* **2006**, *110*, 25568–25572.
32. Hohng, S.; Ha, T. Near-Complete Suppression of Quantum Dot Blinking in Ambient Conditions. *J. Am. Chem. Soc.* **2004**, *126*, 1324–1325.
33. Plakhotnik, T.; Donley, E. A.; Wild, U. P. Single-Molecule Spectroscopy. *Annu. Rev. Phys. Chem.* **1997**, *48*, 181–212.
34. Kumar, P.; Lee, T. H.; Mehta, A.; Sumpter, B. G.; Dickson, R. M.; Barnes, M. D. Photon Antibunching from Oriented Semiconducting Polymer Nanostructures. *J. Am. Chem. Soc.* **2004**, *126*, 3376–3377.
35. Hollars, C. W.; Lane, S. M.; Huser, T. Controlled Non-Classical Photon Emission from Single Conjugated Polymer Molecules. *Chem. Phys. Lett.* **2003**, *370*, 393–398.
36. Yu, J.; Hu, D. H.; Barbara, P. F. Unmasking Electronic Energy Transfer of Conjugated Polymers by Suppression of O-2 Quenching. *Science* **2000**, *289*, 1327–1330.
37. Jaiswal, J. K.; Mattoussi, H.; Mauro, J. M.; Simon, S. M. Long-Term Multiple Color Imaging of Live Cells Using Quantum Dot Bioconjugates. *Nat. Biotechnol.* **2003**, *21*, 47–51.
38. Derfus, A. M.; Chan, W. C. W.; Bhatia, S. N. Intracellular Delivery of Quantum Dots for Live Cell Labeling and Organelle Tracking. *Adv. Mater.* **2004**, *16*, 961–966.